Engineering Structures 248 (2021) 113231

Contents lists available at ScienceDirect

Engineering Structures

journal homepage: www.elsevier.com/locate/engstruct

Iron-Based shape memory alloy for strengthening of 113-Year bridge

Jakub Vůjtěch [a,*], Pavel Ryjáček [a], Jose Campos Matos [b], Elyas Ghafoori [c,d,*]

[a] Faculty of Civil Engineering, Czech Technical University in Prague, Thákurova 7, 166 29 Prague, Czech Republic
[b] ISISE, Department of Civil Engineering, University of Minho, 4800-058 Guimarães, Portugal
[c] Department of Civil and Environmental Engineering, Imperial College London, London SW7 2AZ, UK
[d] Empa, Swiss Federal Laboratories for Material Science and Technology, Überlandstrasse 129, CH-8600 Dübendorf, Switzerland

ARTICLE INFO

Keyword:
Shape memory alloy
Phase transformation
Prestressed strengthening
Bridge
Recovery stress
Repair
Strengthening

ABSTRACT

This study focuses on the large-scale application of a Fe-Mn-Si shape memory alloy (Fe-SMA) for strengthening a historic roadway bridge in Petrov nad Desnou (113-years), Czech Republic. To the best of the authors' knowledge, this is the first application of an iron-based SMA (Fe-SMA) for prestressed strengthening of a bridge. In this study, the shape memory effect (SME) of the Fe-SMA was used for the prestressed strengthening of bridge girders. A mechanical anchorage system was developed to apply multiple Fe-SMA strips to the steel girders of the bridge subjected to daily passengers and heavy trucks. The SME of the Fe-SMA was activated by heating to approximately 260 °C using ceramic heating pads. The test results showed that the recovery stress of the Fe-SMA strips resulted in a compressive stress of approximately –33 MPa in the lower flange of the bridge girder. This compressive stress significantly increased the yield and fatigue capacity of the strengthened girder. Before and after the strengthening, the bridge was loaded with a 45-ton crane to assess the efficiency and performance of the system. Laboratory experiments were performed to optimize the mechanical anchors and examine the feasibility of the proposed strengthening method prior to application to the bridge. Finally, long-term monitoring of the prestressed Fe-SMA plates after installation on the bridge was conducted. The results showed that the main loss of the prestressing force caused by relaxation occurred within the first 30 days after activation and was approximately 20% of the original prestress.

1. Introduction

The aging of historic steel bridges is a global problem. Approximately 70% of steel bridges in Europe are older than 50 years, with 30% being in service for more than 100 years [1]. There are many bridges in the Czech Republic that have reached the end of their design life or have already exceeded 100 years of service [2]. Bridge authorities often seek repair solutions to combat this problem. Repairing existing bridges is often cheaper than replacing the entire structure and helps achieve sustainability by extending the service life [3]. Carbon fiber-reinforced polymer (CFRP) has been used in civil engineering in the past few decades. CFRP materials are effective for repairing existing bridges and buildings [4], and prestressed CFRP can significantly improve the efficiency of CFRP repairs [5,6]. Nevertheless, prestressed members typically require large and complex anchorage systems to transfer forces to the parent member. The placement of hydraulic actuators is also complicated because of the limited space near anchorage devices [7].

1.1. Shape memory alloys (SMAs)

SMAs are smart metallic materials with a beneficial property known as the so-called shape memory effect (SME). The SME enables a material to recover its initial shape after permanent deformation when subjected to a predefined temperature. The first materials with a significant SME were Ni-Ti SMAs, which were developed in the 1960 s. Applications of Ni-Ti alloys were initially reserved for the aviation industry and healthcare. Ternary Ni-Ti-Nb alloys are used in civil engineering, and the addition of Nb increases the yield strength [8], thermal hysteresis, and damping capacity [9] of the Ni-Ti alloy. The applications of Ni-Ti and Ni-Ti-Nb in civil engineering have been focused on the confinement of cracked concrete members [10].

Iron-based shape memory alloys (Fe-SMAs) are suitable for civil engineering applications, mainly because their material characteristics are similar to those of structural steel. Fe-SMAs suitable for civil engineering applications were developed in the 1980s in Japan, and in 1982, a paper [11] on these first Japanese-produced iron-based SMAs was

* Corresponding authors.
E-mail addresses: jakub.vujtech@fsv.cvut.cz (J. Vůjtěch), elyas.ghafoori@empa.ch (E. Ghafoori).

https://doi.org/10.1016/j.engstruct.2021.113231

Available online 25 September 2021

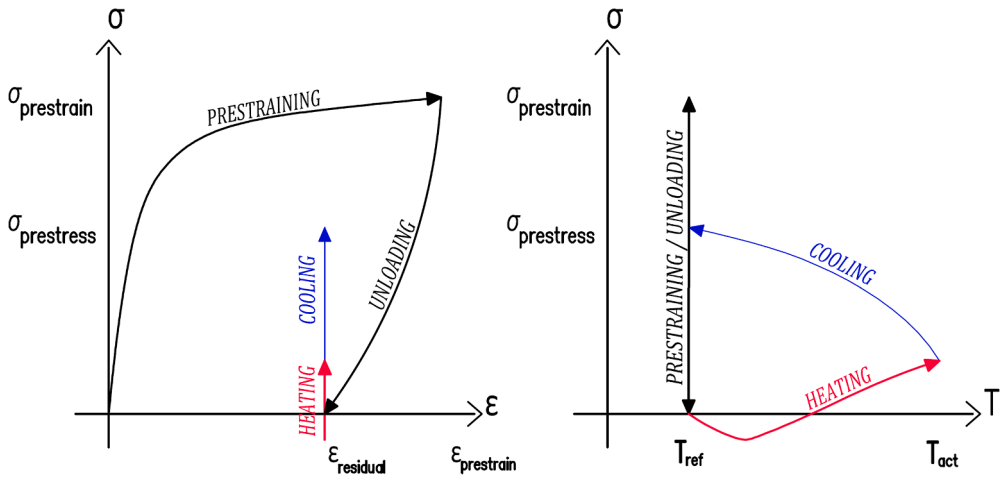

Fig. 1. Fe-SMA strengthening principle.

published. It should be noted that the overall production cost of Fe-SMA is significantly lower than that of Ni-Ti SMA [12].

As the most promising material for prestressing steel bridge members, Fe-SMAs developed at the Swiss Federal Laboratories for Materials Science and Technology (Empa) [13] were used to strengthen the Petrov bridge. Empa's Fe-SMA has been developed in recent years and has shown potential for efficient applications in civil engineering. The mechanical properties and production procedure of the latest alloy composition (used in this study) are described in [14]. Empa's Fe-SMA is currently manufactured in the shape of Ø18 bars and 120 mm × 1.5 mm plates. Thus far, their use was mainly focused on reinforcing concrete "building structures," as presented in [15]. Empa's Fe-SMA was first used for strengthening a bridge in July 2019 in the Czech Republic.

1.2. Strengthening principle

The proposed strengthening method focuses on using the SME of prestrained Fe-SMA for the post-tensioning of critical members. The main principle of Fe-SMA strengthening (Fig. 1) is described in the following section.

After production, the received Fe-SMA is prestrained to a permanent strain of 2.5%. The deformed Fe-SMA is then anchored to the parent structure, thus preventing it from returning to its original length. The Fe-SMA is heated to an activation temperature and subsequently allowed to cool to the ambient temperature. During the entire activation procedure (heating and subsequent cooling), Fe-SMA develops a prestressing force that returns the material to its original shape. Izadi et al. [16] measured the resulting stress in Fe-SMA at 406 MPa upon activation to 260 °C. Until now, Fe-SMA strips have been developed and used for the fatigue strengthening of steel plates [17,18], girders [19,20], and bridge connections [21].

1.3. Fe-Mn-Si SMA for prestressed strengthening

Many applications of this cost-effective Fe-SMA [22-24] demonstrate its potential for use as an effective prestressing element without the need for heavy and complex prestressing equipment [25]. Since then, Fe-SMAs have been used for strengthening steel [17,18,26,27] and concrete [28] structures. Several studies on the mechanical properties of Fe-SMA, including its fatigue [24], cyclic [29], fire [30], and recovery stress [8] behavior, have been conducted.

Studies on the application of Fe-SMA to strengthening steel

Fig. 2. Historic steel road bridge in Petrov nad Desnou, Czech Republic.

(a) (b)

Fig. 3. a) Lower chord joint and b) lower flange of cross-beam.

structures are in the pioneering stage, as only the findings of a few related studies have been published in the literature. Izadi et al. [26,31] developed a Fe-SMA system for strengthening steel plates using a new friction-based clamping system (a mechanical anchor). Thermal activation with a maximum temperature of 260 °C was achieved through electrical resistive heating. This process resulted in recovery stresses of 350–400 MPa. The activated (prestressed) Fe-SMA yielded a maximum compression of −74 MPa in the steel member. This Fe-SMA strengthening technique has also been applied to the fatigue strengthening of cracked steel plates, significantly improving the fatigue life and preventing fatigue crack propagation in some cases [17].

In addition to and in conjunction with studies on the SMA strengthening of steel plates, Izadi et al. [18] adapted a specially designed flat prestressed unbonded reinforcement system for the flexural strengthening of a steel girder with activated Fe-SMA strips. The Fe-SMA strips were activated to maximum temperatures of 100, 160, and 260 °C, resulting in recovery stresses of 161, 328, and 431 MPa, and compressive stresses of −10.7, −21.9, and −28.8 MPa, respectively, in the bottom flange of the girder. The retrofitted steel beam was then subjected to static and fatigue four-point bending tests. The test results indicated a significant increase in the static and fatigue performance of the steel girders [18]. Adhesively bonded joints have recently been used to connect Fe-SMA strips to steel substrates [32]. It has been shown that small Fe-SMA patches adhesively bonded to steel details can arrest fatigue cracks [15,33]. A comparative study on the mechanical and structural performance of Fe-SMA has been conducted [7].

1.4. Outline of study

An application of a Fe-SMA for strengthening the historic steel bridge in Petrov nad Desnou, Czech Republic (Fig. 2) is proposed in this paper. To the best of the author's knowledge, this study is the first-ever application of SMA strengthening to a bridge structure. Petrov Bridge was constructed in 1906 on an arterial road of the Czech Republic and has still been in service (after 113 years) during the proposed Fe-SMA strengthening. Two main factors were considered during the strengthening design: first, the capacity of the member and its influence on the global capacity of the bridge and, second, how widely the member is used in various historic steel bridges. One of the cross girders of the bridge was selected for the strengthening application because it is an ideal representative of a riveted I-beam and a critical member. The Fe-SMA was applied to minimize the effects of traffic loads.

2. Case study structure

The investigated bridge was a steel truss bridge with a span of 19.50 m. The bridged obstacle was river Desna, and the superstructure was skewed at 52° and rested on two monolithic concrete supports. Similar to other steel structures built before the second half of the 20th century, the joints were connected through riveting.

Riveted structures are typically prone to corrosion degradation because of inappropriate details, dirt, and water; this was also the case for the Petrov bridge. Bridge inspections showed that the main weakness of the structure was the reduction of the cross-sections, owing to

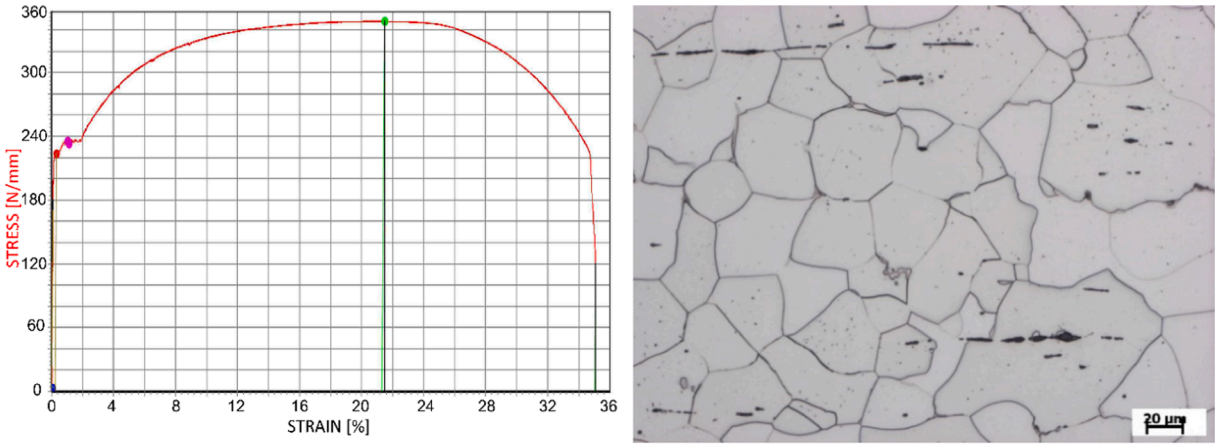

(a) (b)

Fig. 4. a) Tensile test and b) metallography of the reference steel sample extracted from the bridge.

Table 1
Characteristic values of structural yield stress of plate and angle samples.

Yield stress of angles (MPa)	Yield stress of plates (MPa)
280	233

corrosion. The worst situations were observed for the joints of the lower chord of both main truss girders and the lower flange of the cross-beams (Fig. 3).

Because of its relevance to the overall capacity factor, one of the cross-beams was selected for strengthening. The selected beam is an ideal representative sample of a riveted I-beam found in many bridges.

The global corrosion of a structure is usually the leading cause of subsequently defected and weakened members. The best approach to prevent the need for strengthening in similar cases is through the regular inspection and systematic restoration of anticorrosion coating.

The characteristics of the structural steel were defined from the material samples, that is, plates and angles, of the parent structure. The characteristics were analyzed through metallography, spectroscopy, and tensile testing. When the samples were removed, we aimed to minimize the intervention in the parent structure and its static function. The typical characteristics of the plate sample are shown in Fig. 4. Its metallography shows a ferritic structure with cementite particles at the edges of the grains. The structure contained slight plastic inclusions of sulfide and phosphide.

The characteristic value of the yield stress of the structural steel was determined according to *ISO 13822: Bases for the design of structures - Assessment of existing structures*. Table 1 lists the yield stress values of the plates and angles.

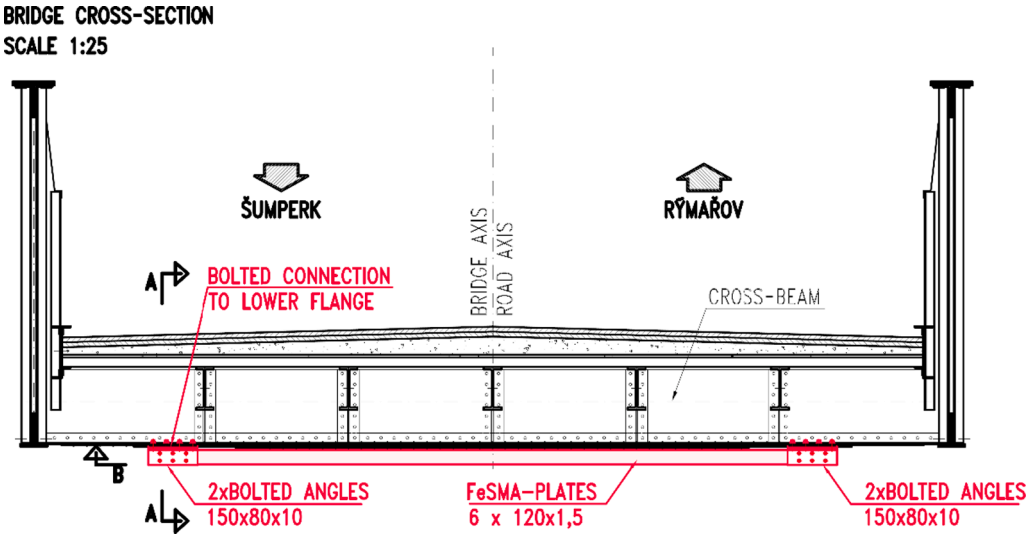

Fig. 5. Cross-section of Petrov bridge strengthened with the Fe-SMA strips.

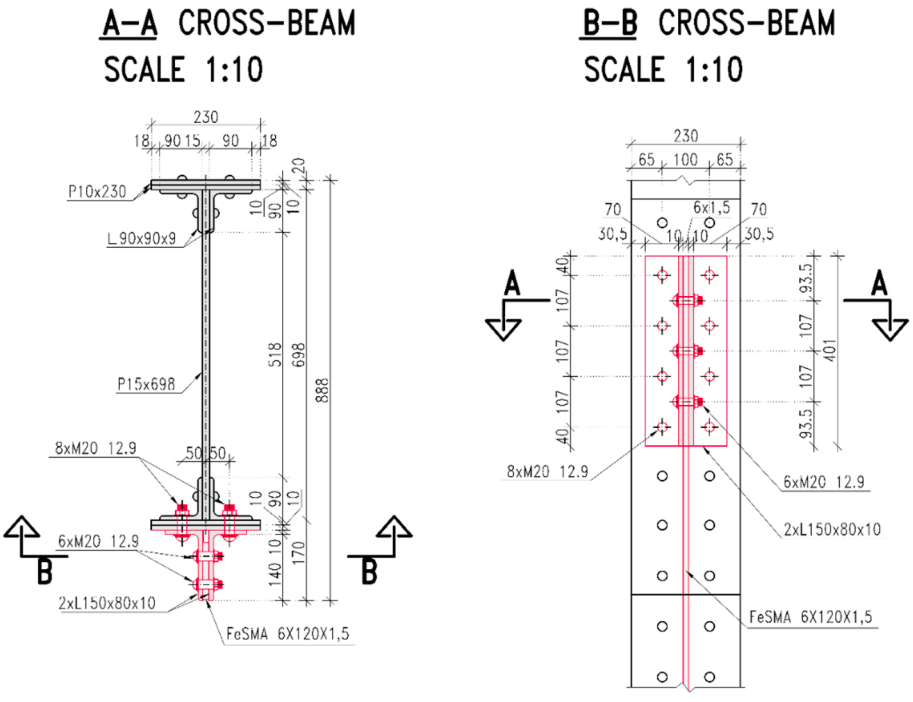

Fig. 6. Details of the anchorage system used to attach prestressed Fe-SMA strips to the bridge girder.

Table 2
Mechanical properties of Fe-SMA strips.

Elastic modulus (GPa)	Poisson's ratio (-)	Yield stress (MPa)	Ultimate strength (MPa)	Activation temperature (°C)	SME prestress (MPa)	Substitute thermal expansion ratio (K^{-1}) *
173	0.3	546	1015	260	406	9.03E-06

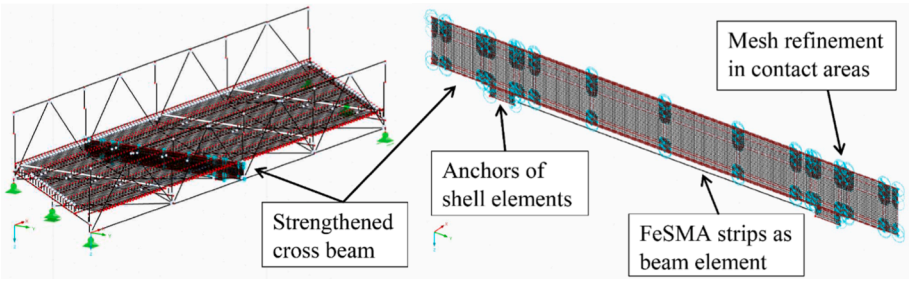

Fig. 7. Numerical simulation of Petrov bridge with shell elements used for the cross-beam.

3. Design of retrofit strengthening system

It is challenging to connect the strengthening member to the historic structure. Ideally, the connection should be completely reversible and should not cause any permanent intervention in the historical parent structure [22].

The Fe-SMA was installed at the bottom flange of the cross beam, as shown in Fig. 5. Several unbonded Fe-SMA plates were used for strengthening because of the limited range of profiles in the market. Fe-SMA plates with a 120 mm × 1.5 mm cross-section were placed between two steel angles of L150 mm × 80 mm × 10 mm dimensions and were bolted with high-strength friction grip (HSFG) bolts M20 12.9 of the high-resistance calibrated (HRC) system, as shown in Fig. 6. Instead of drilling new holes into the cross-beam, holes from several old loose rivets were used for the new bolts. Round-headed HRC bolts were used to ensure visual continuity with the riveted connections on the other parts of the bridge. Thus, the impact of the intervention on the parent structure was reduced to the minimum.

In this case, strengthening was designed to resist traffic loads and increase the fatigue capacity of the strengthened member. The targeted strengthening effect of this experimental application was to achieve permanent compression in the bottom flange of the cross-beam to improve its fatigue resistance. Based on this criterion, six Fe-SMA plates were connected and used. The number of plates required for the targeted strengthening effect was established through preliminary calculations and verified using a numerical model of the entire bridge.

3.1. Activation process

As mentioned in Section 1.2, the activation of the SME involves heating and cooling the material. Various heating methods can be used for this purpose. Electrical resistive heating (ERH) [18] and infrared heating (IR) techniques [16] have been used in previous studies. The main feature of the ERH method is the rapid and uniform heat distribution along the Fe-SMA member. However, its use has been mainly limited to laboratory testing because of the potential risk of leaking electricity to the rest of the steel structure.

For field activation, a new method using ceramic heating pads with a resistance wire was designed. Activation was achieved by heating the Fe-SMA with closely fitted ceramic pads and insulation material. Compared to the ERH and IR techniques, the advantage of this method is that it is energy-efficient, and thus, favorable for field applications. Unlike for ERH, the electrical insolation of the parent steel structure is not required. Heating using ceramic pads and insulation coating was adopted because it is the most suitable technique for activating Fe-SMAs under field conditions.

3.2. Numerical model and material properties

The Fe-SMA properties were provided by the manufacturer, re-fer AG. The substitute thermal expansion ratio of the Fe-SMA was determined based on the expected magnitude of the SME for an activation temperature of 260 °C using **Eq. (1)**. The mechanical properties used for the numerical analysis are listed in Table 2.

$$^{*}\alpha_{SMA} = \frac{\sigma_{SMA}}{E_{SMA}\cdot\Delta^{T}} = \frac{406}{173000\cdot 260} \tag{1}$$

A numerical model of the Petrov bridge (Fig. 7) was used to determine the effects of strengthening on the structure. The model was established using Dlubal RFEM version 5.20 software.

The bridge model comprised beam and shell members with elastic material properties. Four-node S4 shell elements, each with a maximum finite length of 25 mm, were used to simulate the strengthened cross-beam to obtain precise results. The anchoring angles were also modeled using four-node shell elements. The Fe-SMA was represented by a beam member with assigned dimensions and variable width, depending on the number of Fe-SMA plates used. Prestressing was simulated using a uniform temperature load of the Fe-SMA. The dead load, including the self-weight of the steel structure and the upper estimate of the weight of the deck, generated + 32 MPa tensile stress in the bottom flange at the midspan of the cross-girder.

The first simplified estimate of the required number of Fe-SMA plates on a simply supported beam was calculated, and five Fe-SMA plates were required. In this case, the simplification was not precise because of the interaction between the bridge deck and the stringers, as well as the boundary conditions. The actual number of Fe-SMA plates required in the numerical model was verified, considering the interaction and boundary conditions.

The results showed that the designed Fe-SMA strengthening using six 120 mm × 1.5 mm plates was sufficient to resist the dead load with a compressive stress of approximately 35 MPa in the lower flange. Numerical simulations indicated that the activation of the Fe-SMA plates to 260 °C ensured permanent compressive stress in the bottom flange of the cross-girder under dead loads.

4. Experimental program

Before onsite application, laboratory analysis of the designed retrofit

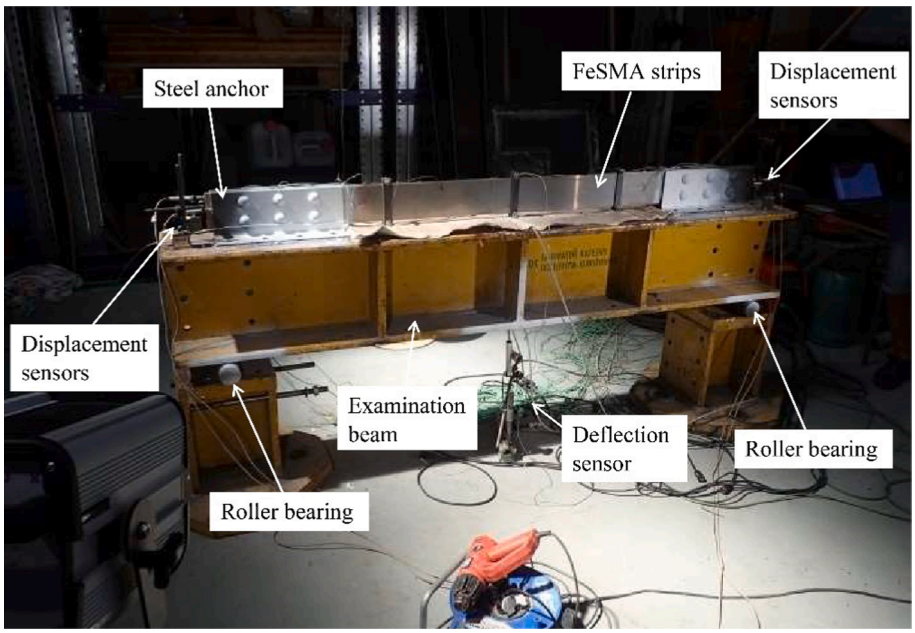

Fig. 8. Experimental setup.

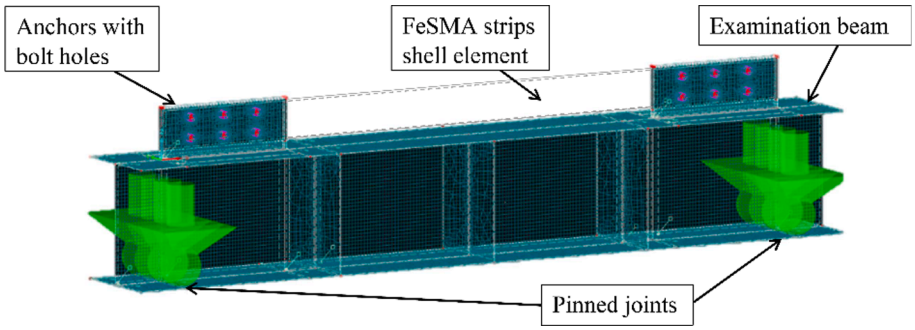

Fig. 9. FE model of the laboratory setup.

strengthening system was conducted in the experimental facility of Czech Technical University in Prague. The aim of the preliminary testing was to verify the reliability of the designed anchorage and activation procedure. The test setup, as shown in Fig. 8, consisted of an examination beam laid on a couple of roller supports and an upper flange mounted with the designed strengthening setup. The strengthening on the upper flange was installed to achieve enhanced accessibility under laboratory conditions.

The same retrofit system designed for the bridge application was used for laboratory testing. The only difference with the bridge application was the number of Fe-SMA plates used. Only two prestrained Fe-SMA plates ready for activation were used for the experimental tests.

4.1. Finite element (FE) simulations

Dlubal RFEM was used to generate a model of the laboratory test beam. The numerical model was composed of only shell elements (Fig. 9). An activation temperature of 260 °C was not achieved during laboratory testing; therefore, the activation temperature in the numerical model of the test beam decreased from 260 to 200 °C.

The model consisted of a laboratory beam with anchors and Fe-SMA plates. The Fe-SMA was modeled using a beam element. The roller bearings were represented by a linear pinned support. The SME was modeled using the substitute thermal expansion ratio as a negative temperature variation of −200 °C. The stress obtained from simulated activation of Fe-SMA to 200 °C in the numerical model in the upper flange was compression of −11.63 MPa.

4.2. Test procedure

The first activation of Fe-SMA was achieved at approximately 200 °C instead of 260 °C. Heating was stopped because of the rapid increase in temperature measured on two thermocouples (more than 350 °C). Therefore, the test was stopped to prevent a possible irreversible change in the material, and an average value of 200 °C was recorded by the other thermocouples.

The following parameters were determined during the experiment (using a sampling frequency of 10 Hz):

- The deflection in the midspan of the experimental beam;
- The slippage of the Fe-SMA plates and anchorage angles;
- The strain on the edges of the upper and lower flanges of the beam;
- The temperature of the Fe-SMA plates.

The experimental setup was mounted using potentiometers, strain gauges, and thermocouples (Fig. 10).

Activation was continued until the Fe-SMA cooled to the ambient temperature. The entire activation process took approximately 2 h from the beginning of the heating. During the cooling phase, a visible difference between the prestrained and non-prestrained plates was

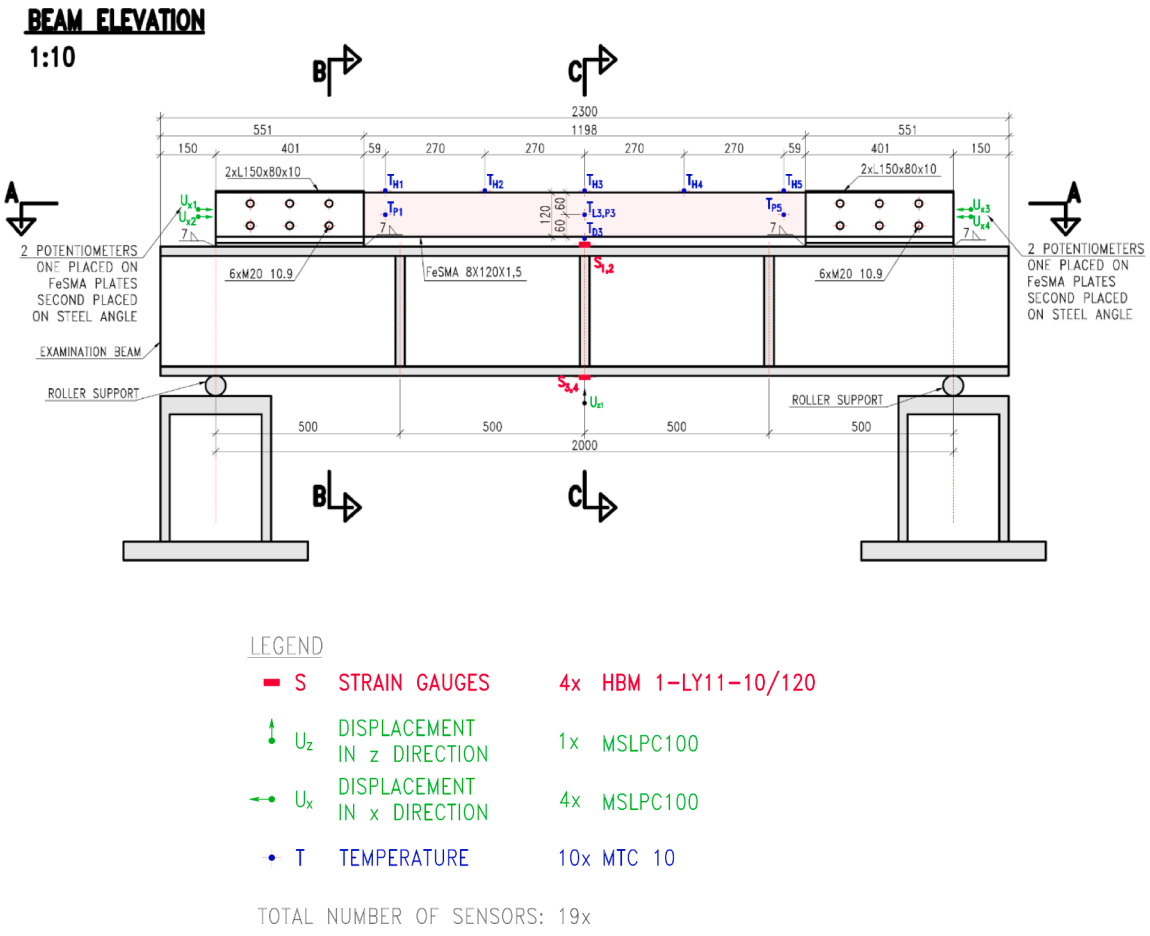

Fig. 10. Setup for the laboratory activation tests.

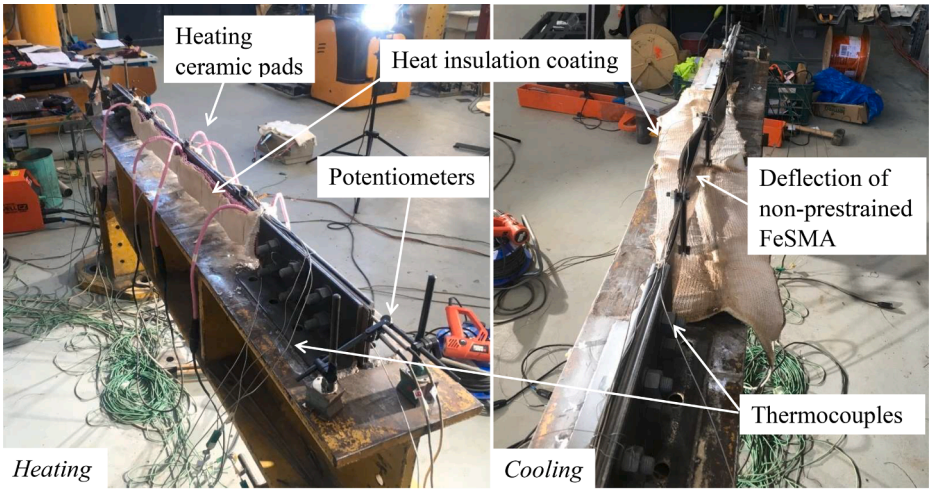

(a) (b)

Fig. 11. (a) Laboratory setup during heating and (b) cooling processes.

observed, as shown in Fig. 11.

4.3. Test results

The change in the Fe-SMA temperature and the stress generated during and after activating the experimental beam were evaluated. The measured values of slippage were at the border of the sensitivity of the potentiometers (0.01 mm), and the measurement conditions for the deflection of the beam were the same. Fig. 12 shows the Fe-SMA temperature during the activation process. The heating was stopped after approximately 20 min, and the cooling of the Fe-SMA occurred for another 100 min. The temperatures recorded by thermocouples TP1 and TP5 increased more rapidly than those by the others because these thermocouples did not attach properly to the Fe-SMA strips but touched

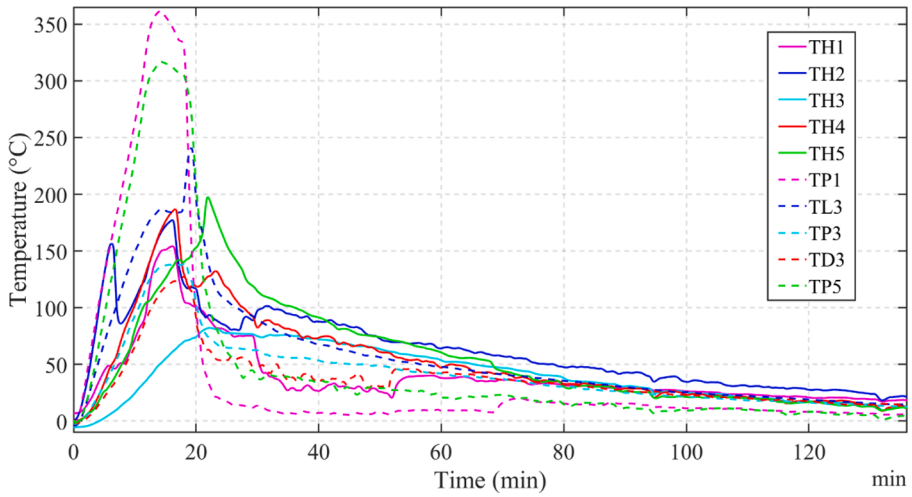

Fig. 12. Temperature-history of the Fe-SMA strips during laboratory activation test (see Fig. 10 for the locations of different thermocouples, T_h).

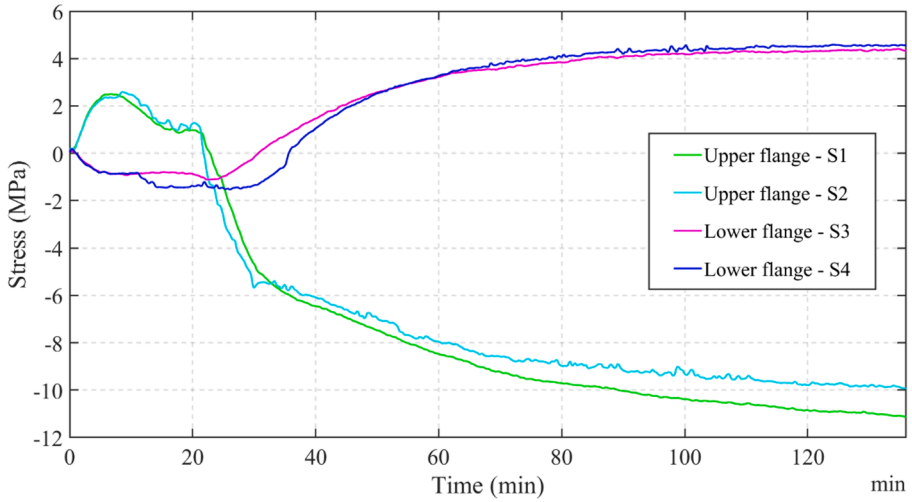

Fig. 13. Stress-history in the midspan of the beam during the laboratory activation test (see Fig. 10 for the locations of different strain gauges, S).

Table 3
Results of the laboratory beam test.

Stress values of laboratory beam with activated Fe-SMA						
Location	Strain gauge	Before activation	Experimental test: After activation	Numerical model: After activation	Direction	[-]
Upper flange	S1	0	−11,55	−11,63	Pressure	MPa
	S2	0	−9,93			MPa
Lower flange	S3	0	4,62	2,54	Tension	MPa
	S4	0	4,62			MPa

the heating pads. This occurrence was observed when the insulation was removed from the strengthening. The stress values were calculated using the stress equation **Eq. (2)**:

$$\sigma_{mid-span} = \varepsilon_{data} \cdot E_{steel} \tag{2}$$

Young's modulus of steel E_{steel} was assumed to be 210 000 MPa. Fig. 13 shows the stress at the midspan of the experimental beam induced during activation. The first sign of the SME was observed after 6 min of heating, with the temperature of the FeSMA plates at approximately 100 °C.

A comparison between the stress values of the cross-beam obtained before and after experimental Fe-SMA activation and the simulation values obtained using the numerical model is presented in Table 3.

The experimental analysis demonstrated the reliability of the retrofit system for application to an actual bridge. The activation method using ceramic heating pads was evaluated and proved to be effective under laboratory conditions. The Fe-SMA was heated to 200 °C for approximately 9 min. The entire activation procedure from the beginning of heating to the complete cooling of the Fe-SMA to the ambient temperature took 1 h 20 min.

5. Fe-SMA strengthening of Petrov bridge

The Fe-SMA was applied to Petrov Bridge in June 2019 without any

Fig. 14. Installation of the Fe-SMA plates on the lower flange of the bridge girder.

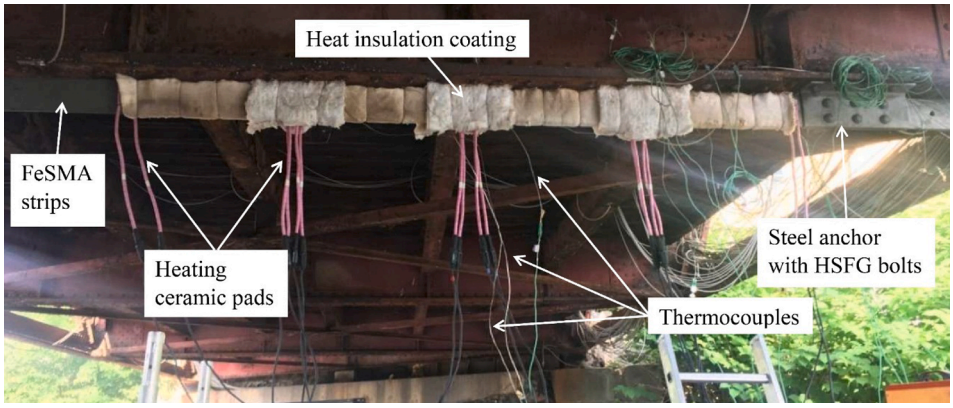

Fig. 15. Heating of the second half of the Fe-SMA strips.

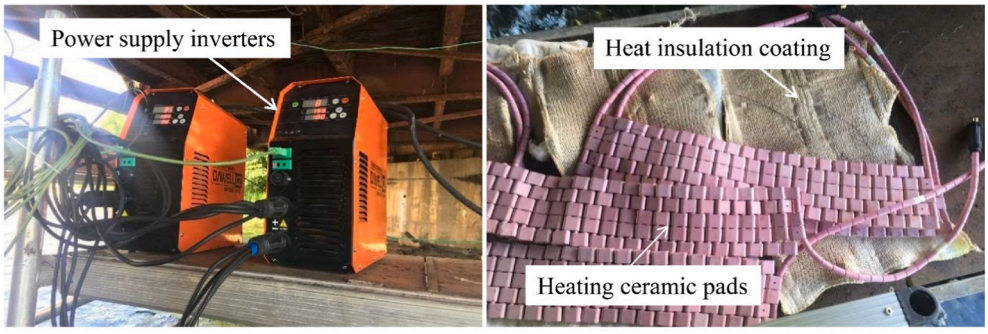

Fig. 16. a) Power supply inverters and b) the ceramic heating pads with the insulation coating.

interference in the traffic on the bridge. The Fe-SMA plates were installed from a small temporary scaffold erected under the bridge for this application. The rivets in the location of the anchors were removed and replaced with HSFG bolts of the HRC system connecting the Fe-SMA plates to the bottom flange of the cross-girder. The activation of the Fe-SMA plates occurred subsequently.

Old loose rivets in the lower flange of the cross-beam located in place of the anchors were hammered out first. Fe-SMA plates bolted at each end between the two angles were placed on the lower flange, as shown in Fig. 14. Holes matching the hammered rivets were drilled into the anchor angles and bolted together. The anchorage system is simple with minimal intervention into the parent structure and offers complete reversibility.

5.1. Activation

The activation process was performed in two steps. Half of the Fe-SMA plates were activated in each step (Fig. 15) because of the limited number of ceramic heating pads available for activation. The power supply was generated using two inverters, as shown in Fig. 16. The inverters controlled the temperature gradient.

In each step, the Fe-SMA plates were sandwiched between ceramic heating pads and wrapped in insulation coating. After installing the ceramic pads and coating, the Fe-SMA plates were heated to a maximum

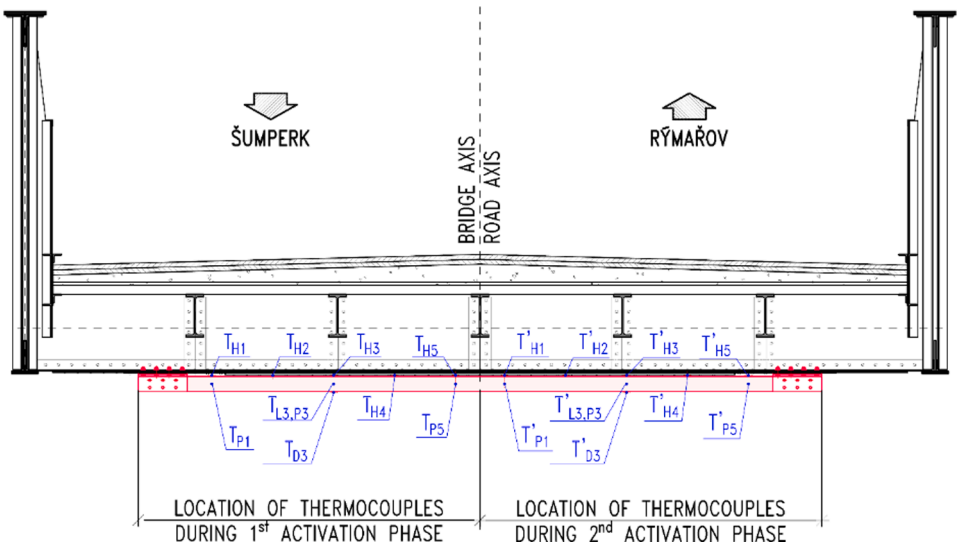

Fig. 17. Locations of the thermocouples along the Fe-SMA strips during the activation steps.

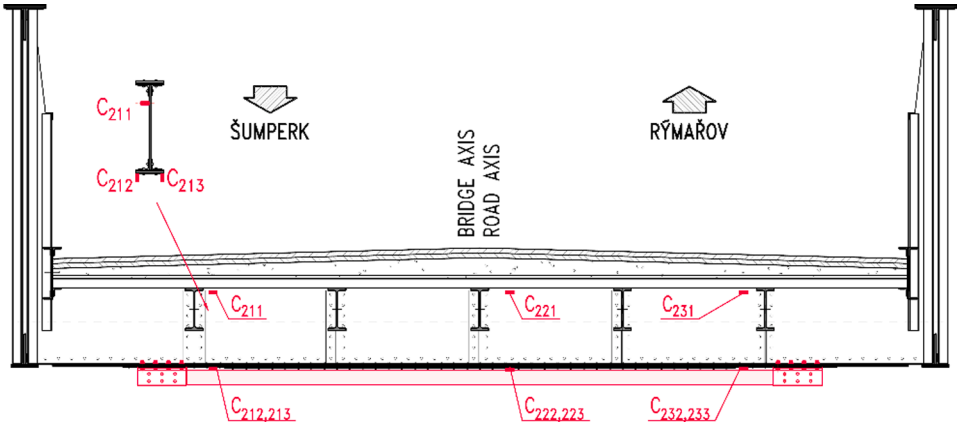

Fig. 18. Layout of the strain gauges on the strengthened bridge girder.

Fig. 19. Final configuration of SMA-strengthened girder in Petrov Bridge.

activation temperature of 260 °C. The temperature was determined using a preliminary numerical model. The temperature of the Fe-SMA and the strain values across the cross-girder were monitored during both activation steps.

5.2. Monitoring

The temperature and its development along the Fe-SMA plates were monitored using ten thermocouples during each activation step, as shown in Fig. 17. The thermocouples were placed along the plates to ensure heating uniformity. During the strengthening of the Petrov bridge, the same layout used in the laboratory tests was applied.

The effect of the Fe-SMA strengthening on the cross-girder was determined using strain gauges placed at three cross-beam sections – at the thirds from both ends of the beam and the midspan of the beam. For each measured cross-section, two strain gauges were placed on each side

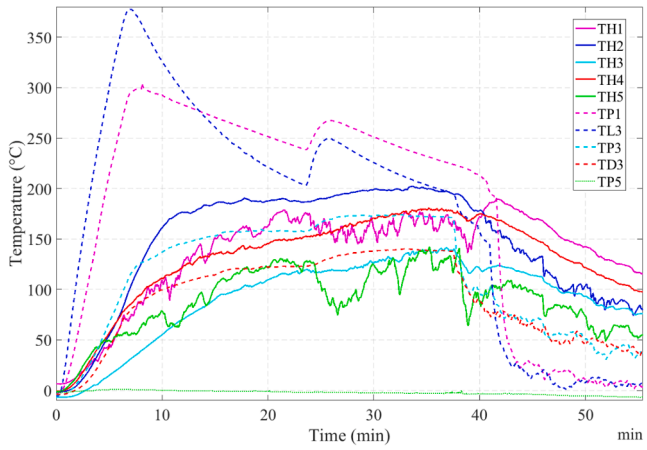

Fig. 20. Temperature-history curves of the Fe-SMA strips (used for bridge strengthening) during the first activation step (see Fig. 17 for the locations of thermocouples, T_h).

of the bottom flange, and one gauge was placed on the web, as shown in Fig. 18.

The Fe-SMA was activated at 260 °C. The final state of the activated Fe-SMA plates on the bridge is shown in Fig. 19. Monitoring was performed during both activation steps.

5.3. Field activation results

The temperature of the Fe-SMA and the strains of the cross-beam were monitored during both activation steps.

Figs. 20 and 21 show the Fe-SMA temperatures during heating and subsequent cooling. Thermocouple T_{P5} was eliminated during the evaluation of both activation steps because it malfunctioned.

The temperatures recorded by the two thermocouples increased more rapidly than temperatures obtained by the other thermocouples, as was observed during the laboratory activation (in this case, thermocouples TP1 and TL3). The heating was stopped after approximately 40 min. During the cooling process of the Fe-SMA, the heating pads and thermocouples were transferred to the position for the second activation step.

The next phase involved activating the second half of the Fe-SMA. The heating of the second part of the Fe-SMA started approximately 4

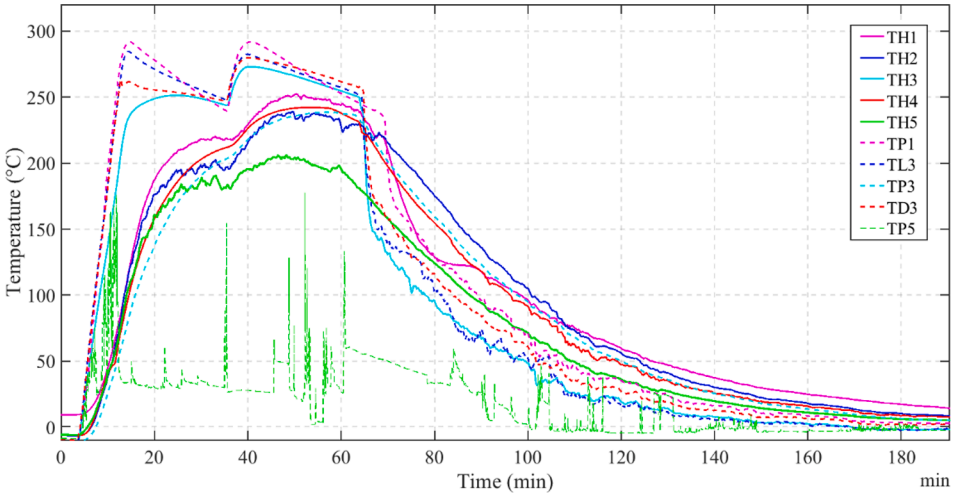

Fig. 21. Temperature-history curves of Fe-SMA strips (used for bridge strengthening) during second activation step (see Fig. 17 for the locations of thermocouples, T_h).

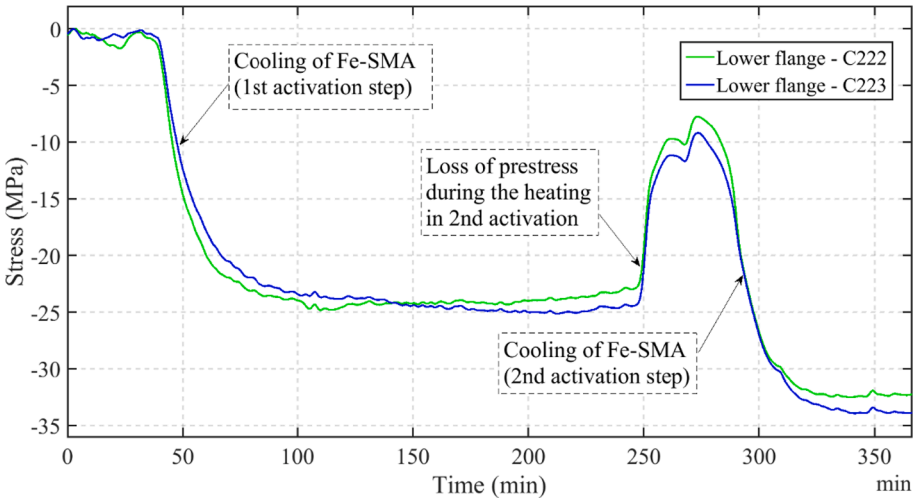

Fig. 22. Stress-history curves at the midspan of the strengthened cross-beam of the bridge during both activation steps (see Fig. 18 for the locations of strain gauges, C).

Table 4
Strengthening effects on cross-girder of Petrov Bridge: experimental and numerical results.

Cross-girder		Strain gauge	Strengthening effect			Numerical model	Units
Section	Part		1st activation	2nd activation	Total		
	Lower flange	C222	−24.78	−7.77	−32.55	−35.273	[MPa]
		C223	−25.20	−8.62	−33.82	−35.273	[MPa]

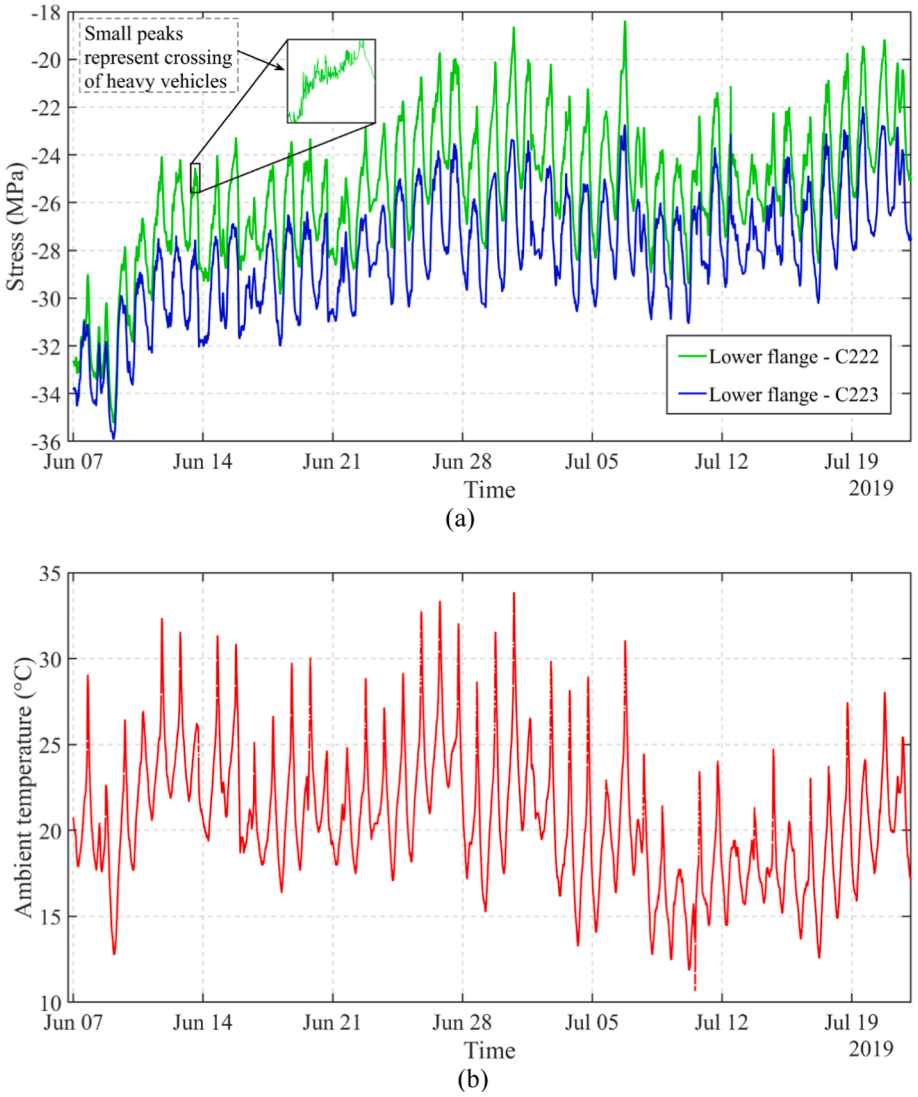

Fig. 23. (a) Long-term monitoring of the stress-history at the midspan of strengthened cross-beam after strengthening (see Fig. 18 for the locations of strain gauges, C). (b) Long-term monitoring of ambient temperature-history at the midspan of the strengthened cross-beam after strengthening.

h after starting the first activation step. The experience gained from the previous activations and the proper installation of the thermocouples, heating pads, and coating guided the experimental precision. In the second activation step, the heating was significantly more uniformly distributed than during both previous activations (the laboratory experiment and the first activation step). The second activation occurred for approximately 3 h, that is, 1 h of heating and 2 h of cooling.

A sign of SME reactivation was observed 30 min after activation commenced. All measured locations showed similar temperature increments. The second activation step was stopped when the average value of all the thermocouples was approximately 260 °C.

In terms of the strengthening effect, the critical values were obtained from the strain gauges in the midspan of the cross-girder. Strain gauges C222 and C223 were placed on the bottom flange of the cross-girder. This section presents a summary of the achieved strengthening effect and a comparison of the results with the numerical model results of Petrov Bridge. Fig. 22 shows the stress state of the midspan during the first and second activation steps. It should be noted that the stress values were reset to zero. Appendix A provides additional information on the stress-history at different locations of the strengthened cross-beam of the bridge during both activation steps.

The strengthening effect of the cross-girder from each activation step and the overall effect are presented in Table 4. A comparison between the overall strengthening effect and the numerical model results of Petrov Bridge is also presented in Table 4.

It was observed that the strengthening effect of the first activation of the SME was significantly higher than that of the second activation. The strengthening effect magnitude of the second activation was

Table 5
Relaxation of the prestressing during the first 42 days after activation of the Fe-SMA plates.

Strain gauge	After strengthening	Elapsed time					Units
		1 day	7 days	14 days	30 days	42 days	
C222	−32.55	−31.94	−27.78	−26.80	−25.13	−25.35	[MPa]
	0.0%	1.9%	14.7%	17.7%	22.8%	22.1%	[-]
C223	−33.82	−32.92	−30.54	−29.00	−27.67	−27.34	[MPa]
	0.0%	2.7%	9.7%	14.3%	18.2%	19.2%	[-]

approximately one-third of that of the first activation, owing to the significant prestress loss during the secondary heating. The results obtained using the numerical model were verified to be accurate compared to the actual stress on the strengthened structure.

5.4. Long-term relaxation of Fe-SMA prestressing

The activated Fe-SMA was monitored until the end of July 2019. The prestress loss of activated Fe-SMA caused by relaxation under laboratory conditions is approximately 10% [34]. The relaxation of the Petrov Bridge strengthening was evaluated based on the stress state of the lower

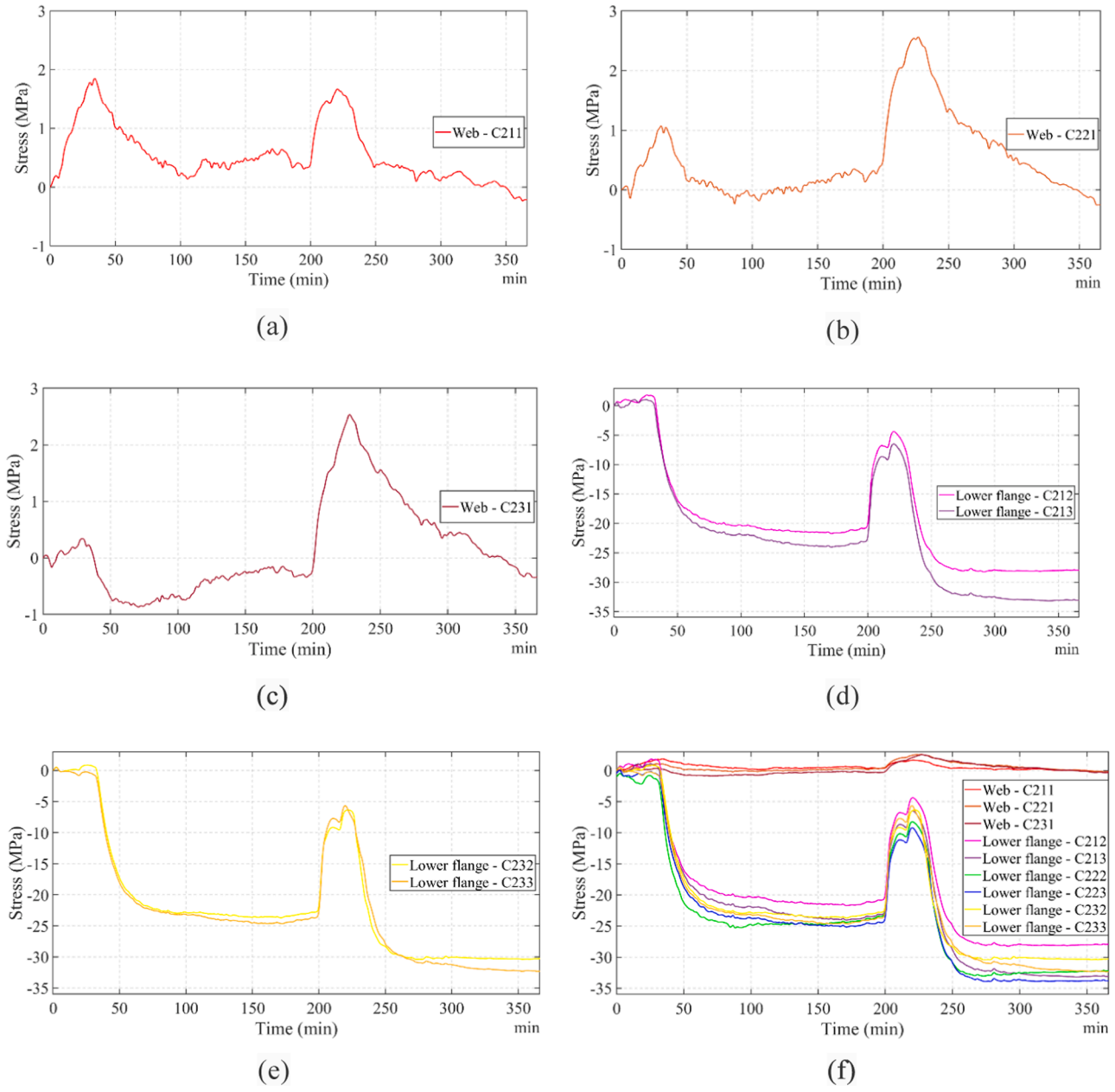

Fig. A1. Stress-history curves of the strengthened cross-beam of the bridge during both activation steps at different locations for (a) Web-C211, (b) Web-C221, (c) Web-C231, (d) Lower flanges – C212 and C213, (c) Lower flanges – C232 and C233, and (f) comparison between all strain gauges (see Fig. 18 for the locations of strain gauges).

flange of the strengthened cross-girder. The stress history of the cross-girder during the first two months after strengthening is depicted in Fig. 23. The stress values were consistent with the final strengthening effect, as described in the previous section.

The slight peaks of the stress values represent the heavy vehicles crossing the bridge. The fluctuation of the stress was consistent with the ambient temperature variations during the day and night. The prestress loss caused by SME relaxation was evaluated based on the average values of the stresses calculated for each day. The day average stress values and the overall prestress loss attributed to relaxation are listed in Table 5.

The results indicated that the main loss of the prestressing force induced by relaxation occurred within the first 30 days after activation and was approximately 20% of the original prestress achieved after activation. Additional factors that could have decreased the prestress level were the live loads from the heavy traffic and the slip of the Fe-SMA strips in the anchor area.

6. Conclusion and remarks

A new type of strengthening with prestressing Fe-SMAs was successfully developed and applied to a 113-year historic steel road bridge in the Czech Republic. Laboratory experiments verified the functionality of the proposed method for strengthening steel bridges. A new activation method was developed using ceramic heating pads and successfully applied to activate the strengthening of an actual bridge. Prestressing using ceramic heating pads was shown to be a reliable technique for activating Fe-SMA. Through Fe-SMA strengthening, a permanent compression in the bottom flange of the cross-beam was achieved, counterbalancing the dead load on the structure. The values obtained using the numerical model were consistent with the measured stress values. The long-term monitoring results showed that the main loss of prestressing force generated by relaxation occurred within the first 30 days after activation and was limited to approximately 20% of the original prestress. The relaxation values obtained under laboratory conditions were significantly lower than those monitored in the Petrov Bridge, possibly owing to the cyclic loads generated by live traffic and temperature fluctuations.

CRediT authorship contribution statement

Jakub Vůjtěch: Visualization, Methodology, Conceptualization, Investigation, Formal analysis, Writing – original draft, Writing – review & editing, Software, Validation. **Pavel Ryjáček:** Supervision, Conceptualization, Project administration, Funding acquisition, Data curation, Validation. **Jose Campos Matos:** Supervision, Validation. **Elyas Ghafoori:** Supervision, Writing – review & editing, Validation.

Declaration of Competing Interest

The authors declare that they have no known competing financial interests or personal relationships that could have appeared to influence the work reported in this paper.

Acknowledgments

The authors are grateful to the Ministry of Culture of the Czech Republic for funding the research work within the framework of the Program of Applied Research and Development of the National and Cultural Identity (NAKI-II) project: Methods for achieving sustainability of industrial heritage steel bridges, ID: DG18P02OVV033. The authors also thank the re-fer AG Company for providing materials used for this study.

Appendix A. . Stress-histories of the bridge girder after strengthening

This appendix provides additional information on the stress-history at different locations of the strengthened cross-beam of the bridge during both activation steps, see Fig. A1.

References

[1] Ghafoori E, Motavalli M, Nussbaumer A, Herwig A, Prinz GS, Fontana M. Design criterion for fatigue strengthening of riveted beams in a 120-year-old railway metallic bridge using pre-stressed CFRP plates. Compos B Eng 2015;68:1–13.
[2] Ryjáček P, Macho M, Stančík V, Polák M. Deterioration and assessment of steel bridges. Monitoring, Safety, Risk and Resilience of Bridges and Bridge Networks: Maintenance; 2016. p. 347.
[3] Ghafoori E. Editorial for special issue on Sustainable Metallic Structures. Eng Struct 2019;183:83.
[4] Vůjtěch J, Ryjáček P, Vovesný M. The numerical analysis of deteriorated steel elements reinforced with CFRP. Adv Trends Eng Sci Technologies 2017;II:303–8.
[5] Hosseini A, Ghafoori E, Motavalli M, Nussbaumer A, Zhao XL, Al-Mahaidi R. Flat Prestressed Unbonded Retrofit System for Strengthening of Existing Metallic I-Girders. Compos B 2018;155:156–72.
[6] Kianmofrad F, Ghafoori E, Elyasi MM, Motavalli M, Rahimian M. Strengthening of metallic beams with different types of pre-stressed un-bonded retrofit systems. Compos Struct 2017;159:81–95.
[7] Hosseini A, Michels J, Izadi M, Ghafoori E. A comparative study between Fe-SMA and CFRP reinforcements for prestressed strengthening of metallic structures. Constr Build Mater 2019;226:976–92.
[8] Wei Liu, Xinqing Zhao. Mechanical Properties and Transformation Behavior of NiTiNb Shape Memory Alloys. Chinese J Aeronautics 2009;22(5):540–3. https://doi.org/10.1016/S1000-9361(08)60138-7. ISSN 1000-9361.
[9] Zhen-zhen Bao, Shun Guo, Fu Xiao, Xin-qing Zhao. Development of NiTiNb in-situ composite with high damping capacity and high yield strength. Prog Nat Sci: Mater Int 2011;21(4):293–300. https://doi.org/10.1016/S1002-0071(12)60060-4. ISSN 1002-0071.
[10] Choi E, Chung Y-S, Choi J-H, Kim H-T, Lee H. The Confining Effectiveness of NiTiNb and NiTi SMA Wire Jackets for Concrete. Smart Mater Struct 2010;19(3):035024. https://doi.org/10.1088/0964-1726/19/3/035024.
[11] Sato A, Chishima E, Soma K, Mori T. Shape memory effect in γ- ↔ ε transformation in Fe-30Mn-1Si alloy single crystals. Acta Metall. 1982;30(6):1177–83.
[12] Sato A, Chishima E, Yamaji Y, Mori T. Orientation and composition dependencies of shape memory effect in Fe-Mn-Si alloys. Acta Metall. 1984;32(4):539–47.
[13] Dong Z, Klotz UE, Leinenbach C, Bergamini A, Czaderski C, Motavalli M. A Novel Fe-Mn-Si Shape Memory Alloy With Improved Shape Recovery Properties by VC Precipitation. Adv Eng Mater 2009;11(1-2):40–4.
[14] Lee WJ, Weber B, Feltrin G, Czaderski C, Motavalli M, Leinenbach C. Stress recovery behaviour of an Fe–Mn–Si–Cr–Ni–VC shape memory alloy used for prestressing. Smart Mater Struct 2013;22(12):125037. https://doi.org/10.1088/0964-1726/22/12/125037.
[15] Ghafoori E, Neuenschwander M, Shahverdi M, Czaderski C, Fontana M. Elevated temperature behavior of an iron-based shape memory alloy used for prestressed strengthening of civil structures. Constr Build Mater 2019;211:437–52.
[16] Izadi MR, Ghafoori E, Shahverdi M, Motavalli M, Maalek S. Development of an iron-based shape memory alloy (Fe-SMA) strengthening system for steel plates. Eng Struct 2018;174:433–46.
[17] Izadi MR, Ghafoori E, Motavalli M, Maalek S. Iron-based shape memory alloy for the fatigue strengthening of cracked steel plates: Effects of re-activations and loading frequencies. Eng Struct 2018;176:953–67.
[18] Izadi M, Hosseini A, Michels J, Motavalli M, Ghafoori E. Thermally activated iron-based shape memory alloy for strengthening metallic girders. Thin-Walled Struct 2019;141:389–401.
[19] Fritsch E, Izadi M, Ghafoori E. Development of nail-anchor strengthening system with iron-based shape memory alloy (Fe-SMA) strips. Constr Build Mater 2019;229:117042. https://doi.org/10.1016/j.conbuildmat.2019.117042.
[20] Izadi M, Motavalli M, Ghafoori E. Iron-based shape memory alloy (Fe-SMA) for fatigue strengthening of cracked steel bridge connections. Constr Build Mater 2019;227:116800.
[21] Ghafoori E. 2015. Fatigue strengthening of metallic members using un-bonded and bonded CFRP laminates. PhD Thesis, ETH-Zurich, https://doi.org/10.3929/ethz-a-010453130.
[22] Leinenbach C, Kramer H, Bernhard C, Eifler D. Thermo-Mechanical Properties of an Fe–Mn–Si–Cr–Ni–VC Shape Memory Alloy with Low Transformation Temperature. Adv Eng Mater 2012;14(1-2):62–7.
[23] Leinenbach C, Lee WJ, Lis A, Arabi-Hashemi A, Cayron C, Weber B. Creep and stress relaxation of a FeMnSi-based shape memory alloy at low temperatures. Mater Sci Eng, A 2016;677:106–15.
[24] Ghafoori E, Hosseini E, Leinenbach C, Michels J, Motavalli M. Fatigue behavior of a Fe-Mn-Si shape memory alloy used for prestressed strengthening. Mater Des 2017;133:349–62.
[25] Hosseini E, Ghafoori E, Leinenbach C, Motavalli M, Holdsworth SR. Stress recovery and cyclic behaviour of an Fe–Mn–Si shape memory alloy after multiple thermal activation. Smart Mater Struct 2018;27:025009.

[26] Izadi M., Ghafoori E., Hosseini A., Motavalli M., Maalek S. Development of anchorage systems for strengthening of steel plates with iron-based shape memory alloy strips, in: Fourth Conference on Smart Monitoring, Assessment and Rehabilitation of Civil Structures (SMAR 2017). 2017.
[27] Izadi M, Motavalli M, Ghafoori E. Iron-based shape memory alloy (Fe-SMA) for fatigue strengthening of cracked steel bridge connections. Constr Build Mater 2019;227:116800. https://doi.org/10.1016/j.conbuildmat.2019.116800.
[28] Shahverdi M, Michels J, Czaderski C, Motavalli M. Iron-based shape memory alloy strips for strengthening RC members: Material behavior and characterization. Constr Build Mater 2018;173:586–99.
[29] Rosa DIH, Hartloper A, de Castro e Sousa A, Lignos DG, Motavalli M, Ghafoori E. Experimental behavior of iron-based shape memory alloys under cyclic loading histories. Construct Build Mater 2021;272.
[30] Izadi M., Ghafoori E., Hosseini A., Motavalli M., Maalek S., Czaderski C., Shahverdi M. Feasibility of iron-based shape memory alloy strips for prestressed strengthening of steel plates, in: the fourth International Conference on Smart Monitoring, Assessment and Rehabilitation of Civil Structures (SMAR 2017). 2017.
[31] Wang W, Hosseini A, Ghafoori E. Experimental study on Fe-SMA-to-steel adhesively bonded interfaces using DIC. Eng Fract Mech 2021;244:107553.
[32] Wang W, Li L, Hosseini A, Ghafoori E. Novel fatigue strengthening solution for metallic structures using adhesively bonded Fe-SMA strips: A proof of concept study. Int J Fatigue 2021;148:106237.
[33] Li L, Chen T, Gu X, Ghafoori E. Heat Activated SMA-CFRP Composites for Fatigue Strengthening of Cracked Steel Plates. J Compos Constr 2020;24(6):04020060. https://doi.org/10.1061/(ASCE)CC.1943-5614.0001072.
[34] Leinenbach C, Lee WJ, Lis A, Arabi-Hashemi A, Cayron C, Weber B. Creep and stress relaxation of a FeMnSi-based shape memory alloy at low temperatures. Mater Sci Eng: A 2016;677:106–15. https://doi.org/10.1016/j.msea.2016.09.042.